Ferriprehnite, $Ca_2Fe^{3+}(AlSi_3)O_{10}(OH)_2$, an Fe^{3+} analogue of prehnite, from Kouragahana, Shimane Peninsula, Japan

Mariko NAGASHIMA*, Daisuke NISHIO-HAMANE**, Shuichi ITO* and Takahiro TANAKA***

*Division of Earth Science, Graduate School of Science and Technology for Innovation, Yamaguchi University, Yamaguchi 753-8512, Japan
**The institute for Solid State Physics, the University of Tokyo, Kashiwa 277-8581, Japan
***Nittetsu mining Co., Ltd., Marunouchi 2-3-2, Chiyoda-ku, Tokyo 100-8377, Japan

Ferriprehnite (IMA2020-057), ideal formula $Ca_2Fe^{3+}(AlSi_3)O_{10}(OH)_2$, is a new mineral that was found as secondary mineral in druses developed in the hydrothermal altered dolerite from Kouragahana, Shimane Peninsula, Japan. Ferriprehnite is an Fe analogue of prehnite. The crystals consisting of ferriprehnite and prehnite occur as a radial aggregate. The tabular crystals are up to 300 μm long, 100 μm wide, and 50 μm thick. Ferriprehnite is colorless to pale green with white streak and vitreous luster. It has a Mohs hardness of 6½. Its cleavage is good on {100}. The calculated density is 2.97 g/cm^3. The empirical formula of ferriprehnite on the basis of 10O + 2OH using the result obtained by electron microprobe analysis is $Ca_{1.99}(Fe^{3+}_{0.66}Al_{0.34})_{\Sigma 1.00}(Al_{1.02}Si_{2.98})_{\Sigma 4.00}O_{10}(OH)_2$. Structure refinement converged to $R1 = 4.64\%$. Its space group is orthorhombic *Pma*2 with unit-cell parameters $a = 18.6149(10)$ Å, $b = 5.4882(3)$ Å, $c = 4.6735(3)$ Å, and $V = 477.46(1)$ Å^3. The determined site occupancy at the octahedral *M* site is $Fe_{0.637(9)}Al_{0.363}$ indicating that the *M* site is predominantly occupied by Fe. <*M*-O> increases with increasing Fe content leading to isotropic expansion of MO_6 octahedra. The *a*- and *c*- dimensions of ferriprehnite are longer than those of prehnite due to Fe substitution for Al at the *M* site.

Keywords: New mineral, Ferriprehnite, Prehnite, Fe

INTRODUCTION

Ferriprehnite (IMA2020-057), ideal formula $Ca_2Fe^{3+}(AlSi_3)O_{10}(OH)_2$, is a new mineral that was found as secondary mineral in druses developed in hydrothermal altered dolerite from Kouragahana, Shimane Peninsula, Japan. The Fe-rich prehnite from the same locality described by Kato et al. (1992) seems to be similar to ferriprehnite in the present study. The mineral ferriprehnite is named for prehnite, which has Fe^{3+}-dominant occupancy at the octahedral site. The structural formula of prehnite and ferriprehnite is represented as $^{VII}A_2{}^{VI}M^{IV}T1_2{}^{IV}T2_2O_{10}(OH)_2$ ($Z = 2$). The 7-coodinated *A* site is generally filled with Ca. The octahedral *M* site is dominantly occupied by Al in prehnite and Fe^{3+} in ferriprehnite. There are two crystallographically independent tetrahedral *T*1 and *T*2 sites. The *T*1 site is filled only by Si, whereas the *T*2 site is occupied by both Al and Si. Prehnite is orthorhombic, but the space group depends on the distribution of Al and Si at the *T*2 site (e.g., Papike and Zoltai, 1967 in their figure 3). Different site names were used in previous structural studies of prehnite. Moreover, two different space groups having different setting were applied. To avoid confusion, the site name correspondence, applied space group and setting were summarized in Supplementary Table S1 (available online from https://doi.org/10.2465/jmps.210127). If tetrahedral Al and Si are disordered, the space group is centrosymmetric *Pncm* (Peng et al., 1959, Table S1). However, ordering of Al and Si leads to the noncentrosymmetric space group *P*2*cm* (Table S1, e.g., Preisinger, 1965; Balić-Žunić et al., 1990; Detrie et al., 2008, 2009). This is supported by the experimental results of Papike and Zoltai (1967), who observed weak forbidden reflections for space group *Pncm*. Although the monoclinic space group *P*2/*n* has also been suggested based on the arrangement of the *T*2 tetrahedra (Baur et al., 1990), a successful refinement in space group *P*2/*n* is lacking. As mentioned above, although the space groups *Pncm* and *P*2*cm* have been applied to refine the crystal structures of prehnite in some

doi:10.2465/jmps.210127
M. Nagashima, nagashim@yamaguchi-u.ac.jp Corresponding author

previous studies, both space groups are not standard-settings based on International Tables for Crystallography Vol. A (Hahn, 2002). The setting for space group *Pncm* is obtained by changing the standard setting of ***abc*** in space group *Pmna* to ***bca***, and the setting for space group *P*2*cm* is obtained by changing the standard setting of ***abc*** in space group *Pma*2 to $\bar{\boldsymbol{c}}\boldsymbol{ba}$ (Hahn, 2002). Space groups with standard-setting were applied to investigate to structural characteristics of Fe-rich Kouragahana prehnite (Akasaka et al., 2003). Here we employ the standard setting of the non-centrosymmetric space group *Pma*2 as had been used for Kouragahana prehnite.

The type specimens of ferriprehnite are deposited at the National Museum of Nature and Science, Tsukuba, Japan, and the Geological and Mineralogical Museum of Faculty of Science, Yamaguchi University, Japan, under registered number NSM-M47662 (holotype) and 97216F (cotype), respectively. In the present study, the new mineral from Kouragahana was examined using electron probe microanalysis and X-ray single-crystal diffraction methods. We re-determined also chemical compositions and structures of prehnite specimens from N'Chwaning Mine, South Africa and Sekigawa, Ehime, Japan to guarantee unbiased insight into the effect of Fe^{3+} at octahedral sites on the entire structure.

OCCURRENCE OF FERRIPREHNITE

Ferriprehnite was found at Kouragahana, Shimane Peninsula, Japan. At that site, several secondary minerals such as prehnite, pumpellyite, babingtonite, and thomsonite occur widely in druses developed in the hydrothermally altered dolerite with Miocene age (e.g., Kano et al., 1986). Part of the Miocene dolerite is coarse-grained as a result of hydrothermal alteration, and thus was described as an 'altered gabbroic sill' by Kano et al. (1986). Secondary minerals including Fe-rich prehnite and babingtonite have been reported from these altered rocks, in which they replace primary minerals or fill cavities (Kano et al., 1986; Akasaka et al., 1997, 2003; Nagashima et al., 2016, 2018). Ferriprehnite from Kouragahana occurs as a radial aggregate in close association with fine-grained prehnite, calcite, and thomsonite-Ca (Fig. 1a). The plate-like crystals of ferriprehnite often develop in druses, accompanied by julgoldite (Fig. 1b).

APPEARANCE AND PHYSICAL PROPERTIES

The crystals consisting of ferriprehnite and prehnite occur in tabular shape up to 300 μm long, 100 μm wide, and 50 μm thick. Ferriprehnite forms the core inside the crystal, and its area generally coincides with the plate-like appearance, but it partially shows an irregular shape (Fig. 1). Ferriprehnite is colorless to pale green with white streak and vitreous luster. It has a Mohs hardness of 6½. Its cleavage is good on {100}. The calculated density is 2.97 g/cm^3 using electron microprobe and single-crystal X-ray diffraction data. Pure materials for optical measurements could not be separated from bulk crystal due to its occurrence.

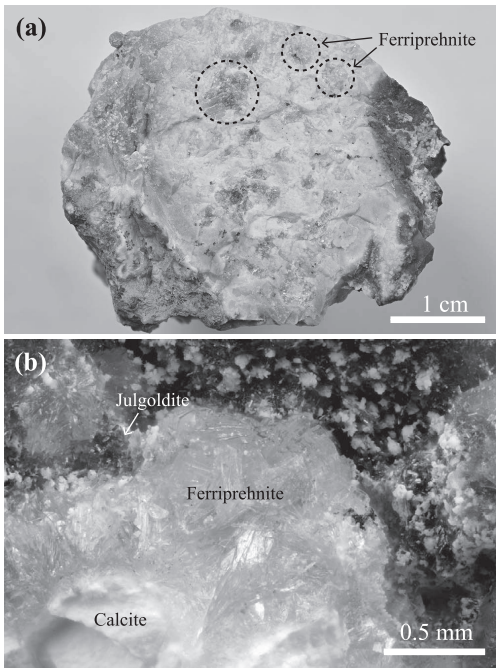

Figure 1. Representative occurrence for ferriprehnite with fine-grained prehnite, calcite and thomsonite-(Ca) (a) and crystal aggregates in a druse (b). Color version is available online from https://doi.org/10.2465/jmps.210127.

EXPERIMENTAL METHODS

Chemical analyses of ferriprehnite and prehnite were performed using an electron probe microanalyzer (EPMA, JEOL JXA-8230) installed at Yamaguchi University, Japan. Chemical compositions of the ferriprehnite, prehnites, and probe standards are listed in Table 1. Operating conditions for EPMA were accelerating voltage of 15 kV, a beam current of 20 nA and a beam diameter of 1-5 μm. Wavelength-dispersion spectra were collected using LiF, PET, and TAP monochromator crystals to identify interfering elements and locate the best wavelengths for background measurements. The ZAF correction-method was used for all elements. H_2O was not directly measured but single crystal XRD refinement revealed the existence of $(OH)^-$ groups. The slightly low total wt% can be due to electron-beam damage and/or voids hidden under the beam spot. Thus, H_2O in wt% was calculated based on

Table 1. Chemical compositions of ferriprehnite and prehnites

	Ferriprehnite		Prehnite				Standards used
	Kouragahana, Shimane Peninsula, Japan		N'Chwaning mine, South Africa		Sekigawa, Ehime, Japan		
	wt% n [1] = 21	Variation	wt% n [1] = 7	Variation	wt% n [1] = 18	Variation	
SiO_2	40.50	39.85-41.13	43.44	43.23-43.80	42.31	41.35-43.05	$CaSiO_3$
TiO_2	0.05	0.00-0.24	0.03	0.00-0.14	0.01	0.00-0.05	TiO_2
Al_2O_3	15.61	13.99-18.52	24.76	24.59-24.87	21.64	18.80-23.54	Al_2O_3
Cr_2O_3	0.01	0.00-0.06	0.01	0.00-0.04	0.01	0.00-0.05	Cr_2O_3
V_2O_3	0.03	0.00-0.09	0.00	0.00	0.18	0.03-0.44	$Ca_3(VO_4)_2$
Fe_2O_3	11.93	7.74-14.17	0.04	0.00-0.10	3.23	0.61-6.60	Fe_2O_3
MnO	0.01	0.00-0.02	0.25	0.10-0.52	0.02	0.00-0.09	MnO
MgO	0.03	0.00-0.13	0.00	0.00	0.00	0.00-0.01	MgO
CaO	25.18	24.75-25.63	26.88	26.74-27.02	26.23	25.94-26.60	$CaSiO_3$
SrO	0.00	0.00	0.00	0.00	0.00	0.00	$SrBaNb_4O_{12}$
BaO	0.02	0.00-0.10	0.01	0.00-0.04	0.02	0.00-0.11	$SrBaNb_4O_{12}$
Na_2O	0.02	0.00-0.05	0.02	0.00-0.09	0.03	0.00-0.06	$NaAlSi_3O_8$
K_2O	0.00	0.00-0.01	0.01	0.00-0.04	0.02	0.00-0.03	$KAlSi_3O_8$
F	0.02	0.00-0.13	0.14	0.03-0.26	0.00	0.00	CaF_2
Cl	0.00	0.00-0.02	0.00	0.00	0.00	0.00-0.01	NaCl
H_2O [2]	4.06		4.36		4.22		
-O = F+Cl	0.01		0.06		0.00		
Total	97.46		99.90		97.93		
Based on 10O + 2OH							
Si	2.98	2.97-3.01	2.99	2.98-3.00	3.00	2.99-3.01	
Ti	0.00	0.00-0.01	0.00	0.00-0.01	0.00	0.00	
Al	1.36	1.22-1.59	2.01	1.99-2.02	1.81	1.61-1.96	
Cr	0.00	0.00	0.00	0.00	0.00	0.00	
V^{3+}	0.00	0.00-0.01	0.00	0.00	0.01	0.00-0.03	
Fe^{3+}	0.66	0.43-0.79	0.00	0.00-0.01	0.17	0.03-0.36	
Mn^{2+}	0.00	0.00	0.01	0.01-0.03	0.00	0.00-0.1	
Mg	0.00	0.00-0.01	0.00	0.00	0.00	0.00	
Ca	1.99	1.97-2.02	1.98	1.97-1.99	1.99	1.96-2.01	
Sr	0.00	0.00	0.00	0.00	0.00	0.00	
Ba	0.00	0.00	0.00	0.00	0.00	0.00	
Na	0.00	0.00-0.01	0.00	0.00-0.01	0.00	0.00-0.01	
K	0.00	0.00	0.00	0.00	0.00	0.00	
Total	6.99		7.00		7.00		
F^-	0.00	0.00-0.01	0.00	0.00	0.00	0.00	
Cl^-	0.00	0.00	0.03	0.01-0.06	0.00	0.00	

[1] Number of analytical points.
[2] Calculated.

the stoichiometry.

The X-ray diffraction data of ferriprehnite and prehnite single crystals were collected using a Bruker SMART APEX II CCD diffractometer installed at Shimane University, Japan. Crystals were mounted on a glass fiber, and intensity data were measured at room temperature using graphite-monochromatized Mo$K\alpha$ radiation (λ = 0.71073 Å). Preliminary lattice parameters and an orientation matrix were obtained from twelve sets of frames and refined during the integration process of the intensity data. Diffraction data were collected with ω scans at different φ settings (φ-ω scan) (Bruker, 1999).

Data were processed using SAINT (Bruker, 1999). An empirical absorption correction using SADABS (Sheldrick, 1996) was applied. The reflection statistics and systematic absences were consistent with the non-centrosymmetric space group *Pma*2. Structural refinement was performed using SHELXL-97 (Sheldrick, 2015). Scattering factors for neutral atoms were employed (Prince, 2004). The site occupancies of the *A* and *T*1 sites were refined with Ca and Si without restraints in preliminary refinement, respectively. They turned out to be fully-occupied within standard deviation in all specimens. Thus, the *A* and *T*1 sites were assumed fully occupied by Ca and Si, respectively. The *M* site was refined with scattering factors of Fe and Al. The site occupancy of the *M* site in N'Chwaning prehnite was fixed at unity with Al because it turned out to be fully occupied by Al within standard deviation in a preliminary refinement. The *T*2 site is divided into two crystallographically independent sites, *T*2S and *T*2A. Although both Si and Al are distributed at the *T*2S and *T*2A sites, Si and Al are difficult to distinguish due to their similar scattering factors. However, tetrahedral Si and Al can easily be discriminated by their different <*T*2-O> bond-lengths. Thus, based on preliminary refinements occupancy factors at the *T*2S and *T*2A were fixed at unity with Si and Al, respectively. Positions of the hydrogen atoms of the hydroxyl groups were derived from difference-Fourier syntheses and were refined by assuming half occupancy with fixed $U^{iso} = 0.05$ Å^2. In addition, O-H distance was restrained at 0.98 ± 0.02 Å (Franks, 1973).

A simulated powder diffraction pattern of ferriprehnite with Cu*K*α radiation was obtained using RIETAN-FP (Izumi and Momma, 2007) based on the unit-cell parameters and atomic parameters from the single-crystal analysis as the amount of sample was insufficient for powder XRD measurement. In addition, the heterogeneity of our sample did not allow collecting pure ferriprehnite data as a single phase.

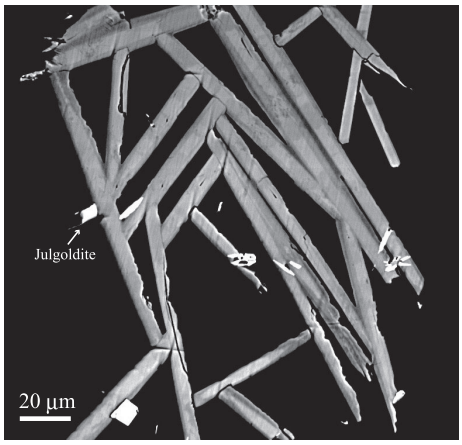

Figure 2. Back-scattered image of ferriprehnite associated with julgoldite. In ferriprehnite, Fe-enriched core (bright) is overgrown with Al-enriched rim (dark).

CHEMICAL DATA

The chemical compositions of ferriprehnite and prehnites are listed in Table 1 with respective standards for elements. Chemical variation of ferriprehnite characterized by Al ↔ Fe^{3+} substitution is observed (Fig. 2). The Fe_2O_3 content attains up to 14.2 wt% corresponding to 0.79 atoms per formula unit (apfu) (Table 1), which is close to the Fe-rich prehnite containing 15.3 wt% Fe_2O_3 reported by Kato et al. (1992) from the same locality. The empirical formula of ferriprehnite on the basis of 10O + 2OH using the result of obtained by EPMA (Table 1) is

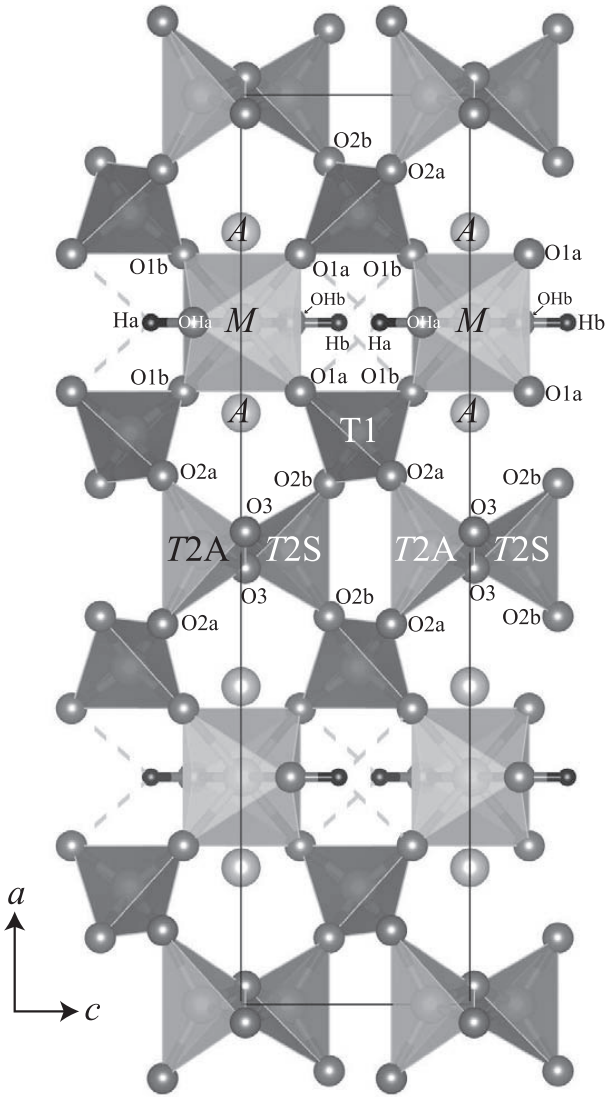

Figure 3. Crystal structure of ferriprehnite projected down [010] drawn with VESTA3 (Momma and Izumi, 2011).

Table 2. Experimental details of the single-crystal X-ray diffraction analysis of ferriprehnite and prehnites

		Ferriprehnite	Prehnite	
Locality		Kouragahana, Shimane Peninsula, Japan	N'Chwaning mine, South Africa	Sekigawa, Ehime, Japan
Fe content		0.637 apfu	-	0.155 apfu
Crystal size (mm)		0.10 × 0.08 × 0.03	0.32 × 0.14 × 0.03	0.07 × 0.03 × 0.02
Space group		*Pma*2	*Pma*2	*Pma*2
Cell parameters	*a* (Å)	18.6149(10)	18.4626(4)	18.5030(6)
	b (Å)	5.4882(3)	5.4793(1)	5.4814(1)
	c (Å)	4.6735(3)	4.6201(1)	4.6346(1)
	V (Å^3)	477.46(1)	467.38(1)	470.05(1)
D_{calc} (g/cm^3)		2.97	2.93	2.95
θ_{min}-θ_{max}(°)		1.1-36.3	2.2-37.8	3.7-38.3
μ (mm^{-1})		2.509	1.865	1.855
Collected reflections		3003	5102	6568
Unique reflections		1408	1928	2446
Completeness d > 0.6 Å		100%	100%	100%
R_{int} (%)		2.62	2.37	2.26
R_σ (%)		3.76	2.82	3.11
Index ranges		-30≤*h*≤31, -9≤*k*≤6, -2≤*l*≤7	-31≤*h*≤30, -8≤*k*≤9, -7≤*l*≤7	-31≤*h*≤32, -9≤*k*≤9, -8≤*l*≤8
*R*1 (%)		4.71	2.49	2.89
w*R*2 (%)		10.16	6.40	6.31
No. of parameters		98	97	98
Weighting scheme		$w = 1/[\sigma^2(F_o^2) + (0.0230P)^2 + 2.69P]$	$w = 1/[\sigma^2(F_o^2) + (0.0266P)^2 + 0.20P]$	$w = 1/[\sigma^2(F_o^2) + (0.0260P)^2 + 0.21P]$
Flack parameter		0.0(2)	0.00(6)	0.00(5)
$\Delta\rho_{max}$ (e Å^{-3})		1.62 at 0.70 Å from *A*	0.67 at 0.60 Å from *A*	0.60 at 0.92 Å from *T*1
$\Delta\rho_{min}$ (e Å^{-3})		-1.25 at 0.65 Å from *M*	-0.54 at 1.77 Å from Ha	-0.60 at 0.48 Å from Hb

Note: The function of the weighting scheme is $w = 1/(\sigma^2(F_o^2) + (a\cdot P)^2 + b\cdot P)$, where $P = [\mathrm{Max}(F_o^2) + 2F_c^2]/3$, and the parameters *a* and *b* are chosen to minimize the differences in the variances for reflections in different ranges of intensity and diffraction angle.

$Ca_{1.99}(Fe^{3+}_{0.66}Al_{0.34})_{\Sigma1.00}(Al_{1.02}Si_{2.98})_{\Sigma4.00}O_{10}(OH)_2$ (analytical number, n = 21). The ideal formula is $Ca_2Fe^{3+}(AlSi_3)O_{10}(OH)_2$, which requires (in wt%) 40.85 SiO_2, 11.55 Al_2O_3, 18.10 Fe_2O_3, 25.42 CaO, 4.08 H_2O, and total 100 wt%. Akasaka et al. (2003) also investigated Fe-bearing prehnite from Kouragahana. Their Fe-bearing prehnite formed spherical aggregate associated with Fe-rich pumpellyite and calcite. This prehnite seems to have formed under higher temperature than our ferriprehnite associated with thomsonite-(Ca). Based on their description, prehnite displayed distinct heterogeneity. Fe-poor prehnite generally grows over clusters of Fe-rich prehnite, or Fe-poor and Fe-rich crystals form mutual intergrowths in the spherical aggregates. The Fe content in the Fe-bearing prehnite studied by Akasaka et al. (2003) varies from 0.07 to 8.08 wt% Fe_2O_3 corresponding to 0.00-0.43 Fe^{3+} apfu. The oxidation state of iron was determined as trivalent using ^{57}Fe Mössbauer spectroscopy (Akasaka et al., 2003). It is interesting that the occurrence and chemical characteristics of Fe-bearing prehnite associated with Fe-rich pumpellyite are considerably different from our ferriprehnite specimens in spite of same locality. Though the coexistence of Fe-rich and Al-rich prehnite was mentioned by Kato et al. (1992), the mineral association of Fe-rich prehnite from the same locality was not described.

Averaged chemical formulae of prehnite from N'Chwaning mine and Sekigawa are $(Ca_{1.98}Mn^{2+}_{0.01})_{\Sigma1.99}Al_{1.00}(Al_{1.01}Si_{2.99})_{\Sigma4.00}O_{10}(OH)_2$ (n = 7) and $Ca_{1.99}(Al_{0.81}$

Table 3. Interatomic distances (Å), *T*-O-*T* angles (°), and deformation parameters

	Ferriprehnite	Prehnite			Ferriprehnite	Prehnite	
	Kouragahana	N'Chwaning mine	Sekigawa		Kouragahana	N'Chwaning mine	Sekigawa
A-O3	2.433(3)	2.422(1)	2.425(1)	*T*1-O1a	1.615(5)	1.607(2)	1.612(2)
A-O2a	2.539(5)	2.528(2)	2.521(2)	*T*1-O1b	1.607(5)	1.610(2)	1.608(2)
A-O2b	2.846(5)	2.802(2)	2.827(2)	*T*1-O2a	1.629(4)	1.636(2)	1.629(2)
A-O1b	2.357(4)	2.366(2)	2.365(1)	*T*1-O2b	1.648(4)	1.652(2)	1.654(2)
A-O1a	2.382(4)	2.379(2)	2.378(1)	$\langle T1\text{-O}\rangle^{IV}$	1.625	1.626	1.626
A-OHa	2.338(4)	2.333(1)	2.334(1)	$\langle\lambda_{tet}\rangle^{1)}$	1.005	1.005	1.005
A-OHb	2.357(4)	2.339(2)	2.339(1)	$\sigma\theta(tet)^{2\,1)}$	19.26	20.97	20.18
$\langle A\text{-O}\rangle^{VII}$	2.465	2.453	2.455				
				*T*2A-O2a (×2)	1.719(4)	1.722(1)	1.730(2)
M-OHa	1.983(5)	1.914(2)	1.930(2)	*T*2A-O3 (×2)	1.728(5)	1.732(2)	1.742(2)
M-OHb	1.977(6)	1.906(2)	1.924(2)	$\langle T2A\text{-O}\rangle^{IV}$	1.724	1.727	1.736
M-O1a (×2)	1.983(5)	1.918(2)	1.934(2)	$\langle\lambda_{tet}\rangle^{1)}$	1.030	1.031	1.031
M-O1b (×2)	1.996(5)	1.923(2)	1.943(2)	$\sigma\theta(tet)^{2\,1)}$	116.00	120.55	119.92
$\langle M\text{-O}\rangle^{VI}$	1.986	1.917	1.935				
$\langle\lambda_{oct}\rangle^{1)}$	1.000	1.001	1.001	*T*2S-O2b (×2)	1.626(5)	1.633(2)	1.623(2)
$\sigma\theta(oct)^{2\,1)}$	1.43	1.56	1.63	*T*2S-O3 (×2)	1.614(5)	1.609(2)	1.600(2)
				$\langle T2S\text{-O}\rangle^{IV}$	1.620	1.621	1.611
OHa...O1a	3.016(7)	3.008(3)	3.018(3)	$\langle\lambda_{tet}\rangle^{1)}$	1.011	1.012	1.012
OHb...O1b	3.012(7)	2.994(3)	2.998(3)	$\sigma\theta(tet)^{2\,1)}$	42.58	47.43	45.55
				*T*1-O2a-*T*2A	136.3(3)	136.47(8)	136.66(8)
				*T*1-O2b-*T*2S	144.5(3)	143.16(12)	144.20(9)
				*T*2S-O3-*T*2A	154.19(19)	154.82(8)	154.55(9)

[1)] $\langle\lambda\rangle$ and $\sigma\theta^2$ are quadratic elongation and angle variance (Robinson et al., 1971).

$Fe^{3+}_{0.17}V^{3+}_{0.01})_{\Sigma 0.99}(Al_{1.00}Si_{3.00})_{\Sigma 4.00}O_{10}(OH)_2$ (n = 18), respectively (Table 1). The N'Chwaning prehnite is relatively homogeneous. On the other hand, in the Sekigawa prehnite the compositional variation is distinct due to Al ↔ Fe^{3+} substitution. The Fe_2O_3 content varies from 0.6 to 6.6 wt% corresponding to 0.03 and 0.36 Fe^{3+} apfu, respectively.

X-RAY CRYSTALLOGRAPHY AND CRYSTAL-STRUCTURE DETERMINATION

Crystallographic data of ferriprehnite and prehnite are summarized in Table 2. The crystal structure of ferriprehnite is shown in Figure 3. Refinements of the structure converged to $R1$ = 4.71% for Kouragahana ferriprehnite, 2.49% for N'Chwaning prehnite and 2.89% for Sekigawa prehnite. Slight chemical heterogeneity of ferriprehnite crystal as shown in Figure 2 may cause the high $R1$ factor. The refined site occupancies, atomic positions, and anisotropic displacement parameters are listed in Appendixes 1

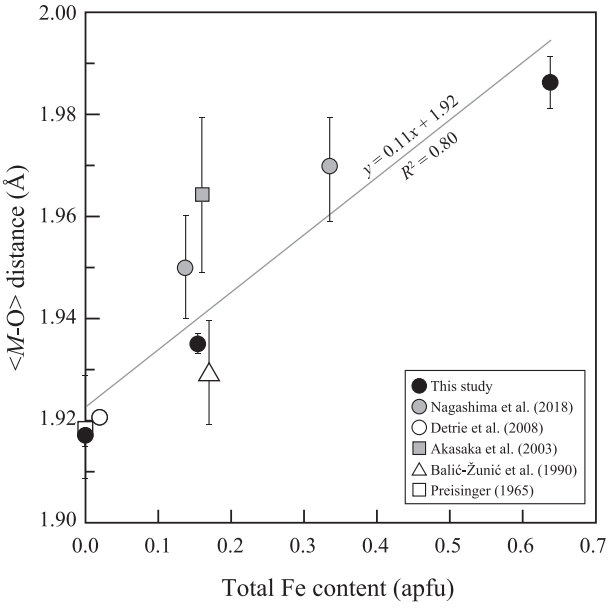

Figure 4. Variation of the <*M*-O> distance (Å) against total Fe content (apfu) in prehnite and ferriprehnite.

and 2, respectively. Two hydrogen positions, Ha and Hb, were determined in this study (Appendix 1). The relationship between donor and acceptor oxygens, and their hydrogen bonds is OHa–Ha···O1a and OHb–Hb···O1b, is consistent with those suggested by Detrie et al. (2008) using TOF neutron Rietveld method. Selected interatomic distances and deformation parameters are listed in Table 3. The simulated powder diffraction pattern of ferriprehnite is listed in Table 4.

Table 4. Simulated powder diffraction pattern based on the result of X-ray single-crystal analysis[1)]

h	*k*	*l*	2θ (°)	*d* cal (Å)	I_{cal}
2	0	0	9.50	9.307	12
1	1	0	16.83	5.264	30
0	0	1	18.97	4.674	32
2	0	1	21.26	4.177	13
0	1	1	25.01	3.558	32
1	1	1	25.47	3.495	54
2	1	1	26.80	3.324	45
4	0	1	27.02	3.298	43
6	0	0	28.75	3.102	9
3	1	1	28.90	3.087	100
4	1	1	31.63	2.827	32
0	2	0	32.61	2.744	5
2	2	0	34.03	2.632	20
6	0	1	34.68	2.585	16
5	1	1	34.85	2.572	77
7	1	0	37.55	2.393	9
0	2	1	37.99	2.366	19
4	2	0	38.04	2.364	17
1	2	1	38.31	2.347	12
6	1	1	38.47	2.338	13
8	0	0	38.66	2.327	12
3	2	1	40.78	2.211	6
7	1	1	42.40	2.130	7
4	0	2	43.29	2.088	8
8	0	1	43.41	2.083	7
4	1	2	46.49	1.952	8
8	1	1	46.60	1.947	11
5	1	2	48.88	1.862	13
9	1	1	51.03	1.788	9
0	2	2	51.31	1.779	45
8	2	0	51.45	1.775	6
6	1	2	51.69	1.767	8
0	3	1	53.77	1.704	8
7	1	2	54.87	1.672	26
8	0	2	55.70	1.649	6
3	3	1	55.93	1.643	8
8	1	2	58.39	1.579	5
12	0	0	59.55	1.551	6
5	3	1	59.64	1.549	21

[1)] Only reflections with relative intensity >5% are listed.

The determined site occupancy at the *M* site is $Fe_{0.637(9)}Al_{0.363}$ for Kouragahana ferriprehnite (Appendix 1) indicating that the *M* site is predominantly occupied by Fe^{3+}. The Fe content is almost consistent with that obtained by chemical analysis (Table 1). The Sekigawa prehnite also contains a small amount of Fe, and the refined site occupancy of the *M* site is $Al_{0.845(3)}Fe_{0.155}$. In contrast, Al^{3+} ions fully occupy the *M* site in N'Chwaning prehnite. Structural variation of prehnite is considered using the data refined in the non-centrosymmetric space group *Pma*2 either in standard setting (this study; Akasaka et al. 2003; Nagashima et al., 2018) or in *P*2*cm* setting (Preisinger, 1965; Balić-Žunić et al., 1990; Detrie et al., 2008). The variation of <*M*-O> increases with increasing Fe content (Fig. 4). In this study, <*M*-O> varies from 1.917 Å (N'Chwaning prehnite) to 1.996 Å (Kouragahana ferriprehnite). Bond-length and angular distortion defined by Robinson et al. (1971) among three specimens are almost constant (Table 3), indicating that the increased Fe content at the *M* site leads to the isotropic expansion of MO_6

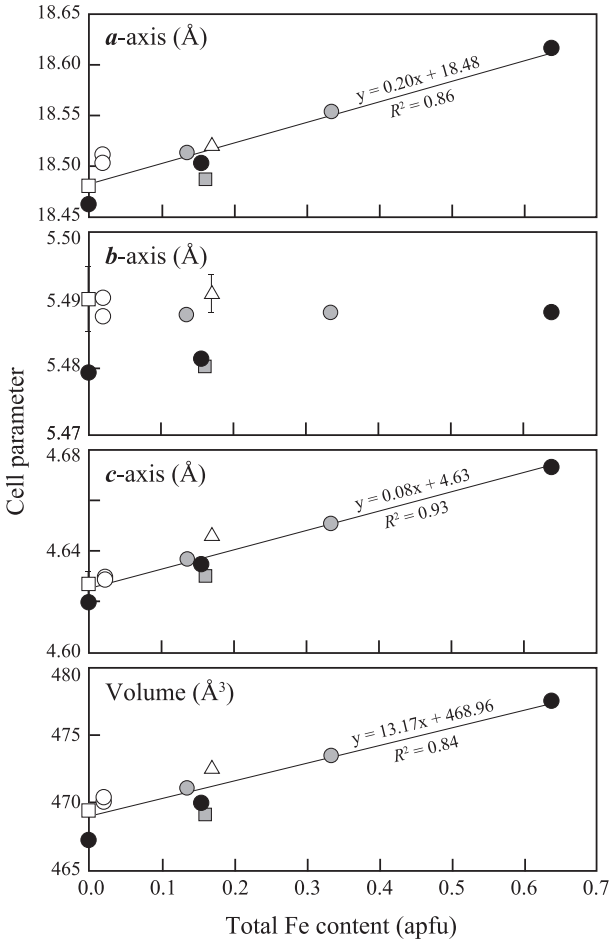

Figure 5. Variation of the unit-cell parameters against total Fe content (apfu) in prehnite and ferriprehnite. Legends are same as those in Figure 4.

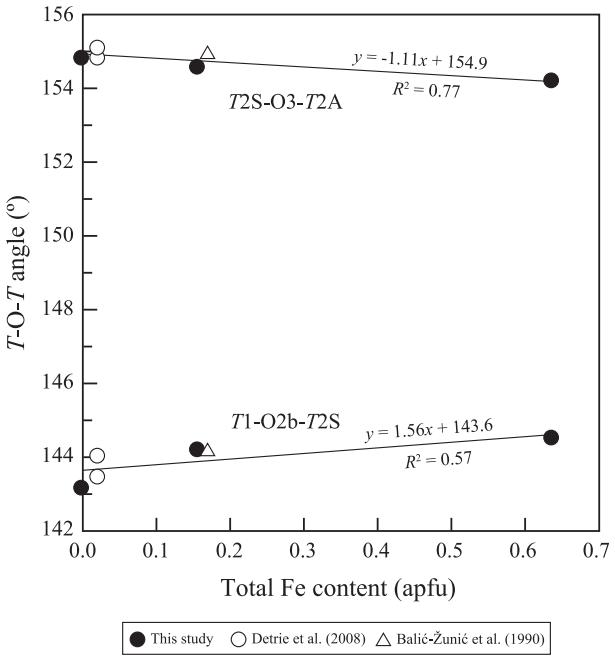

Figure 6. Variation of the *T*-O-*T* angle (°) against total Fe content (apfu) in prehnite and ferriprehnite.

octahedra.

The unit-cell volume of ferriprehnite is much larger than the ones of Al-dominant prehnite due to the difference of octahedral ionic radii: 0.645 Å for Fe^{3+} versus 0.535 Å for Al (Shannon, 1976). The results of the present study and the published ones indicate the positive correlation between the cell volume and Fe content in prehnite (Fig. 5). The increase of the *a*-dimension is more pronounced than that along *c*. However, the *b*-dimension has no correlation with Fe content (Fig. 5). The O1a-O1a' and O1b-O1b' edges of the MO_6-octahedra are oriented along the ***a***-axis and are not constrained by other coordination polyhedra. Thus, an elongation of these edges due to increasing Fe content at the *M* site is directly transferred to the length of the ***a***-axis. The octahedral O1a-O1b edge lies in the *yz*-plane and is ~ 58° inclined to the ***b***-axis but 32° to the ***c***-axis. Consequently, an elongation of the O1a-O1b edge mainly effects the *c*-dimension. The lengths of the remaining octahedral edges terminated by OHa and OHb have no significant effect on the cell dimensions because the hydroxylated octahedral apices participate only in a soft bond to Ca. The minor potential increase of the ***b***-axis with Fe at the *M* site is counterbalanced by a slight reduction of the *T*2S-O3-*T*2A angle and a minor increase of the *T*1-O2b-*T*2S angle (Fig. 6). Thus, as a result, the *b*-dimension is independent of octahedral Fe content.

All of three investigated samples show the same Ca-characteristic <*A*-O> distance of 2.45-2.46 Å and a <*T*1-O> distance of 1.625-1.626 Å referring to a SiO_4 tetrahedron. The <*T*2A-O> and <*T*2S-O> distances are 1.72-1.74 Å and 1.61-1.62 Å, respectively, indicating strong Al preference at the *T*2A site. The difference value (<*T*2A-O> − <*T*2S-O>) gives a clue for the estimation of the order-disorder state of Al and Si at the *T*2 sites. The values in the present study are 0.105 Å for Kouragahana ferriprehnite, 0.106 Å for N'Chwaning prehnite, and 0.125 Å for Sekigawa prehnite. Large difference values indicate stronger Al preference at the *T*2A site. The $T2AO_4$ tetrahedra, in contrast to the $T2SO_4$ tetrahedra, are characterized by severe angular distortion in terms of angle variance, $\sigma\theta(tet)^2$ (Robinson et al., 1971). In a regular SiO_4 tetrahedron with a Si-O bond length of 1.61 Å, the tetrahedral edge is 2.63 Å, which roughly corresponds to 2 × the ionic radius (1.35 Å) of O^{2-} (Shannon, 1976). Thus, the degree of freedom for angular distortion is very restricted. This is contrasted by the larger AlO_4 tetrahedron with an Al-O bond length of ca. 1.75 Å, which has in its regular form an edge-length of 2.86 Å allowing substantial oxygen displacements leading to angular distortion to compensate for structural strain.

ACKNOWLEDGMENTS

Sample collection was permitted by the local manager of a national park, Ms. Nozomi Shionome, in Matsue Ranger Station, Daisen-Oki National Park, Ministry of the Environment. We thank the Editor Dr. T. Kuribayashi, as well as two anonymous reviewers for their constructive comments. We also thank for Prof. Thomas Armbruster for his constructive comments, and Mr. Yoji Morifuku for his technical assistance in using EPMA. This work was supported by JSPS KAKENHI Grant Number JP18K03782 to M.N.

SUPPLEMENTARY MATERIAL

Color version of Figure 1 and Supplementary Table S1 are available online from https://doi.org/10.2465/jmps.210127.

REFERENCES

Akasaka, M., Kimura, Y., Omori, Y., Sakakibara, M. and Togari, K. (1997) ^{57}Fe Mössbauer study of pumpellyite-okhotskite-julgoldite series minerals. Mineralogy and Petrology, 61, 181-198.

Akasaka, M., Hashimoto, H., Makino, K. and Hino, R. (2003) ^{57}Fe Mössbauer and X-ray Rietveld studies of ferrian prehnite from Kouragahana, Shimane Peninsula, Japan. Journal of Mineralogical and Petrological Sciences, 98, 31-40.

Balić-Žunić, T., Šćavničar, S. and Molin, G. (1990) Crystal structure of prehnite from Komiža. European Journal of Mineral-

ogy, 2, 731–734.
Baur, W.H., Joswig, W., Kassner, D. and Hofmeister, W. (1990) Prehnite: Structural similarity of the monoclinic and orthorhombic polymorphs and their Si/Al ordering. Journal of Solid State Chemistry, 86, 330–333.
Bruker (1999) SMART and SAINT-Plus. Version 6.01. Bruker AXS Inc., Madison, Wisconsin.
Detrie, T.A., Ross, N.L., Angel, R.J. and Gatta, G.D. (2009) Equation of state and structure of prehnite to 9.8 GPa. European Journal of Mineralogy, 21, 561–570.
Detrie, T.A., Ross, N.L., Angel, R.J. and Welch, M.D. (2008) Crystal chemistry and location of hydrogen atoms in prehnite. Mineralogical Magazine, 72, 1163–1179.
Franks, F. (1973) Water: A comprehensive treatise, vol. 2. pp. 684, Plenum, New York–London.
Hahn, T. (2002) International Tables for Crystallography. Vol. A: Space-Group Symmetry. Fifth Edition. pp. 911, Springer.
Izumi, F. and Momma, K. (2007) Three-dimensional visualization in powder diffraction. Solid State Phenomena, 130, 15–20.
Kano, K., Satoh, H. and Bunno, M. (1986) Iron-rich pumpellyite and prehnite from the Miocene gabbroic sills of the Shimane Peninsula, Southwest Japan. The Journal of the Japanese Association of Mineralogists, Petrologists and Economic Geologists, 81, 51–58.
Kato, A., Matsubara, S. and Kamiya, T. (1992) Fe^{3+}-analogue of prehnite from Kouragahana, Shimane Prefecture (title is translated from Japanese). Abstract of Annual Meeting of Mineralogical Society of Japan, 160 (in Japanese).
Momma, K. and Izumi, F. (2011) VESTA3 for three-dimensional visualization of crystal, volumetric and morphology data. Journal of Applied Crystallography, 44, 1257–1276.
Nagashima, M, Iwasa, K. and Akasaka, M. (2016) Relation between occurrence and chemical compositions of prehnite in hydrothermally altered dolerite from Mitsu, Shimane Peninsula, Japan. Geoscience Report of Shimane University, 24, 1–8 (in Japanese with English abstract).
Nagashima, M., Iwasa, K. and Akasaka, M. (2018) Oxidation state and distribution of Fe in Fe-rich prehnite in hydrothermally altered dolerite from Shimane Peninsula, Japan: ^{57}Fe Mössbauer and X-ray Rietveld studies. Mineralogy and Petrology, 112, 173–184.
Papike, J.J. and Zoltai, T. (1967) Ordering of tetrahedral aluminum in prehnite. $Ca_2(Al, Fe^{+3})[Si_3AlO_{10}](OH)_2$. American Mineralogist, 52, 974–984.
Peng, S.-T., Chou, K.-D. and Tang, Y.-C. (1959) The structure of prehnite. Acta chimica Sinica, 25, 56–63 (in Chinese).
Preisinger, A. (1965) Prehnit-ein neuer Schichtsilikattyp. Tschermaks Mineralogische und Petrographische Mitteilungen 10, 491–504 (in German).
Prince, E. (2004) International Tables for Crystallography. Volume C: Mathematical, Physical and Chemical Tables. Third Edition. pp. 1000, Kluwer Academic Publishers.
Robinson, K., Gibbs, G.V. and Ribbe, P.H. (1971) Quadratic elongation: a quantitative measure of distortion in coordination polyhedra. Science, 172, 567–570.
Shannon, R.D. (1976) Revised effective ionic radii and systematic studies of interatomic distances in halides and chalcogenides. Acta Crystallographica, A32, 751–767.
Sheldrick, G.M. (1996) SADABS. University of Göttingen, Germany.
Sheldrick, G.M. (2015) Crystal structure refinement with SHELX. Acta Crystallographica, C71, 3–8.

Manuscript received January 27, 2021
Manuscript accepted May 16, 2021

Manuscript handled by Takahiro Kuribayashi

Appendix 1. Site occupancies, atomic positions and thermal parameters of ferriprehnite and prehnites

Site	W[1)]		Prehnite			Site	W[1)]		Ferriprehnite	Prehnite	
			Kouragahana	N'Chwaning mine	Sekigawa				Kouragahana	N'Chwaning mine	Sekigawa
A	4*d*	*x*	0.15047(4)	0.150673(14)	0.150610(17)	O2a	4*d*	*x*	0.0814(2)	0.08263(7)	0.08278(8)
Ca		*y*	0.76165(17)	0.76125(6)	0.76277(6)			*y*	0.0340(6)	0.0288(2)	0.0301(2)
		z	0.0001(10)	0.0000(2)	0.00000(16)			*z*	0.6580(14)	0.6469(4)	0.6501(4)
		U^{eq}	0.00955(16)	0.00801(6)	0.00892(6)			U^{eq}	0.0106(8)	0.0086(3)	0.0099(3)
M	2*c*	*x*	1/4	1/4	1/4	O2b	4*d*	*x*	0.0732(2)	0.07434(8)	0.07353(8)
		y	0.2628(2)	0.26249(14)	0.26432(11)			*y*	0.4581(7)	0.4614(3)	0.4593(2)
		z	0.0068(11)	0.0021(3)	0.0025(2)			*z*	0.3861(14)	0.3851(4)	0.3853(4)
		U^{eq}	0.0054(3)	0.00487(10)	0.00527(14)			U^{eq}	0.0131(8)	0.0115(3)	0.0117(3)
		Occ.	$Fe_{0.637(9)}Al_{0.363}$	$Al_{1.0}$	$Al_{0.845(3)}Fe_{0.155}$	O3	4*d*	*x*	0.02001(15)	0.01969(6)	0.01985(7)
*T*1	4*d*	*x*	0.12876(5)	0.130587(19)	0.13011(2)			*y*	0.7396(7)	0.7402(2)	0.7387(2)
Si		*y*	0.2514(2)	0.25127(9)	0.25127(8)			*z*	0.0189(17)	0.0150(6)	0.0185(5)
		z	0.5138(10)	0.5087(3)	0.5108(2)			U^{eq}	0.0118(6)	0.0103(2)	0.0108(2)
		U^{eq}	0.00665(19)	0.00473(7)	0.00574(7)	OHa	2*c*	*x*	1/4	1/4	1/4
*T*2A	2*a*	*x*	0	0	0			*y*	0.9513(9)	0.9598(3)	0.9592(3)
Al		*y*	0	0	0			*z*	0.7914(9)	0.7951(5)	0.7948(4)
		z	0.8270(10)	0.8164(2)	0.81972(19)			U^{eq}	0.0075(10)	0.0069(3)	0.0088(4)
		U^{eq}	0.0068(4)	0.00514(14)	0.00640(15)	OHb	2*c*	*x*	1/4	1/4	1/4
*T*2S	2*b*	*x*	0	0	0			*y*	0.5754(9)	0.5634(3)	0.5681(3)
Si		*y*	1/2	1/2	1/2			*z*	0.2172(9)	0.2090(5)	0.2105(4)
		z	0.2026(10)	0.1990(2)	0.20048(17)			U^{eq}	0.0098(10)	0.0066(3)	0.0086(3)
		U^{eq}	0.0057(3)	0.00490(12)	0.00598(13)	Ha	2*c*	*x*	1/4	1/4	1/4
O1a	4*d*	*x*	0.1744(2)	0.17654(7)	0.17596(8)			*y*	1.03(2)	0.986(10)	0.989(9)
		y	0.1265(6)	0.1304(2)	0.1311(2)			*z*	0.601(12)	0.5853(18)	0.5863(19)
		z	0.2591(14)	0.2503(4)	0.2514(3)			U^{iso}	0.05	0.05	0.05
		U^{eq}	0.0088(7)	0.0074(2)	0.0088(3)	Hb	2*c*	*x*	1/4	1/4	1/4
O1b	4*d*	*x*	0.1746(2)	0.17667(7)	0.17613(7)			*y*	0.57(2)	0.532(9)	0.538(9)
		y	0.3986(6)	0.3942(2)	0.3970(2)			*z*	0.4267(15)	0.418(2)	0.4189(18)
		z	0.7484(14)	0.7510(4)	0.7494(3)			U^{iso}	0.05	0.05	0.05
		U^{eq}	0.0088(7)	0.0072(2)	0.0080(2)						

[1)] Wyckoff position.

Appendix 2. Anisotropic displacement parameters (Å^2) of ferriprehnite and prehnites

Site		Ferriprehnite	Prehnite		Site		Ferriprehnite	Prehnite	
		Kouragahana	N'Chwaning mine	Sekigawa			Kouragahana	N'Chwaning mine	Sekigawa
A	U^{11}	0.0088(3)	0.00541(10)	0.00719(12)	O1b	U^{11}	0.0125(16)	0.0074(4)	0.0087(6)
	U^{22}	0.0069(3)	0.00728(11)	0.00716(11)		U^{22}	0.0066(13)	0.0089(5)	0.0077(5)
	U^{33}	0.0130(4)	0.01133(13)	0.01240(12)		U^{33}	0.007(2)	0.0054(6)	0.0077(6)
	U^{23}	0.0009(4)	-0.00023(13)	0.00021(12)		U^{23}	-0.0014(13)	-0.0017(5)	-0.0009(4)
	U^{13}	-0.0012(6)	-0.00117(19)	-0.0003(2)		U^{13}	-0.0041(16)	-0.0041(5)	-0.0026(5)
	U^{12}	-0.0001(3)	0.00030(10)	0.00010(12)		U^{12}	0.0002(11)	0.0009(4)	0.0002(4)
M	U^{11}	0.0065(4)	0.0047(2)	0.0058(2)	O2a	U^{11}	0.0101(14)	0.0078(4)	0.0088(6)
	U^{22}	0.0045(4)	0.0059(2)	0.0047(2)		U^{22}	0.0091(13)	0.0084(5)	0.0087(5)
	U^{33}	0.0053(4)	0.0041(2)	0.0053(2)		U^{33}	0.013(2)	0.0095(7)	0.0122(6)
	U^{23}	0.0006(4)	0.0002(2)	0.00028(19)		U^{23}	0.0021(14)	0.0006(5)	0.0008(5)
	U^{13}	0	0	0		U^{13}	0.0042(15)	0.0034(5)	0.0026(5)
	U^{12}	0	0	0		U^{12}	-0.0021(11)	-0.0013(4)	-0.0013(4)
*T*1	U^{11}	0.0074(3)	0.00420(13)	0.00549(16)	O2b	U^{11}	0.0182(18)	0.0107(5)	0.0117(7)
	U^{22}	0.0063(3)	0.00594(15)	0.00567(14)		U^{22}	0.0076(14)	0.0108(6)	0.0091(5)
	U^{33}	0.0063(5)	0.00406(16)	0.00607(15)		U^{33}	0.013(2)	0.0130(7)	0.0141(7)
	U^{23}	-0.0002(4)	0.00002(13)	-0.00007(12)		U^{23}	-0.0029(15)	-0.0001(6)	0.0003(5)
	U^{13}	0.0005(9)	0.0007(3)	0.0000(3)		U^{13}	-0.0031(17)	-0.0052(5)	-0.0050(6)
	U^{12}	0.0001(4)	-0.00010(13)	0.00002(15)		U^{12}	0.0037(12)	0.0041(4)	0.0024(5)
*T*2A	U^{11}	0.0069(9)	0.0040(3)	0.0055(4)	O3	U^{11}	0.0113(10)	0.0091(4)	0.0108(5)
	U^{22}	0.0057(8)	0.0055(3)	0.0059(3)		U^{22}	0.0099(11)	0.0099(4)	0.0090(4)
	U^{33}	0.0077(10)	0.0059(3)	0.0078(3)		U^{33}	0.0142(16)	0.0120(5)	0.0126(5)
	U^{23}	0	0	0		U^{23}	0.0011(13)	0.0028(4)	0.0049(4)
	U^{13}	0	0	0		U^{13}	-0.005(2)	-0.0009(8)	0.0005(7)
	U^{12}	0.0005(6)	-0.0005(2)	-0.0002(3)		U^{12}	-0.0011(11)	0.0000(4)	-0.0002(5)
*T*2S	U^{11}	0.0084(8)	0.0045(2)	0.0062(3)	OHa	U^{11}	0.008(2)	0.0068(6)	0.0105(9)
	U^{22}	0.0042(6)	0.0052(2)	0.0051(2)		U^{22}	0.0069(19)	0.0074(7)	0.0077(7)
	U^{33}	0.0044(8)	0.0050(3)	0.0066(3)		U^{33}	0.007(3)	0.0065(9)	0.0082(8)
	U^{23}	0	0	0		U^{23}	0.0025(18)	0.0000(7)	0.0007(6)
	U^{13}	0	0	0		U^{13}	0	0	0
	U^{12}	0.0009(5)	0.00054(18)	0.0003(2)		U^{12}	0	0	0
O1a	U^{11}	0.0110(15)	0.0079(4)	0.0115(6)	OHb	U^{11}	0.016(2)	0.0092(7)	0.0097(9)
	U^{22}	0.0097(14)	0.0083(5)	0.0074(5)		U^{22}	0.0056(17)	0.0076(7)	0.0083(7)
	U^{33}	0.0056(19)	0.0060(6)	0.0075(6)		U^{33}	0.008(3)	0.0031(8)	0.0078(7)
	U^{23}	0.0002(13)	-0.0011(5)	-0.0009(4)		U^{23}	-0.0005(19)	-0.0010(7)	-0.0002(6)
	U^{13}	0.0013(15)	0.0009(5)	0.0017(5)		U^{13}	0	0	0
	U^{12}	0.0008(11)	-0.0008(4)	-0.0005(4)		U^{12}	0	0	0